Journal of Materials Processing Tech. 324 (2024) 118266

Contents lists available at ScienceDirect

Journal of Materials Processing Tech.

journal homepage: www.elsevier.com/locate/jmatprotec

Characterization and process optimization of remote laser cutting of current collectors for battery electrode production

Caterina Angeloni, Erica Liverani *, Alessandro Ascari, Alessandro Fortunato

Department of Industrial Engineering (DIN), Alma Mater Studiorum - University of Bologna, viale Risorgimento 2, Bologna, Italy

ARTICLE INFO

Associate Editor: Hui-Ping Wang

Keywords:
Laser Cutting
Current Collectors
Battery Production
Copper Foil
Aluminum Foil

ABSTRACT

Aluminum (Al) and copper (Cu) metal foils of thickness 6–20 μm are employed as current collectors for the production of Li-ion battery cathodes and anodes. Greater demand for this product is driving up production rate requirements, especially in the field of car manufacturing. Laser-based cutting processes for trimming and cutting electrodes are considered suitable for meeting this demand as they can achieve very high throughput while maintaining process quality. In order to meet market requirements, laser manufacturers are developing new laser sources, optics, and scanning heads that will improve process productivity and quality. Establishing the relationship between the laser system and cut quality will lead to competitiveness, increased productivity, and sustainability production. This paper presents a thorough analysis of the cutting performance of pulsed and continuous-wave lasers with scanning speeds of up to 28 m/s for processing thin Al and Cu current collectors. Comparisons between process outcomes are made in terms of maximum and minimum cutting speed and power, kerf geometry, cut quality, and presence of defects. Identification of configurations leading to high and low cut quality enables detailed process parameter windows to be defined for both laser system systems employing continuous-wave and pulsed sources. By analyzing correlations between the materials, laser source, and process variables, the main outcome is that continuous-wave single-mode fiber lasers enable highest cut quality in the high-productivity regime, surpassing the current state-of-the-art in laser cutting of metal foils.

1. Introduction

Battery electrode production within the automotive industry currently includes several laser-based manufacturing processes. This is mainly due to the flexibility of laser technology, which can easily be adapted to different battery geometries, as well as its high quality, reliability, and production rate (Pfleging, 2018). The latter is one of the key factors for success of laser applications because of increasing demand from car manufacturers. For simplicity, most lithium-ion batteries have a similar design, including a metal oxide positive electrode (cathode) coated on an aluminum current collector, a carbon/graphite negative electrode (anode) coated on a copper current collector, a separator, and an electrolyte comprising lithium salt in an organic solvent. The final geometry of electrodes is obtained by cutting or trimming the current collectors both within coated and uncoated regions. Aluminum and copper current collectors are 12 μm and 6 μm thick, respectively, and can be cut with satisfactory outcomes both mechanically using knife slitting or die cutting, or thermally using a laser beam. While mechanical cutting exhibits advantages in terms of avoiding defects such as dross adhesion, melting, development of a heat affected zone or spattering, dies require frequent sharpening to prevent burrs, material attachment, and edge bending, which interrupts continuous production and lowers productivity. Laser cutting is instead a non-contact thermal cutting process that combines high production rates in terms of meters of foil cut per second, high levels of flexibility in terms of the range of patterns that can be cut, and high levels of cut quality in terms of minimizing imperfections resulting from laser-material interactions (Banat et al., 2020). There are several papers in the literature that have dealt with laser cutting of electrodes. Lee et al. (2019) evaluated cut characteristics in terms of kerf and melted width of compressed and uncompressed cathodes while varying the scanning speed and volumetric energy. Berhe et al. (2022) identified the main physical phenomena involved in laser cutting and factors affecting cutting efficiency, developing a mathematical model for top, kerf, clearance, and burr widths. Lutey et al. (2015) applied five different laser sources to cutting of $LiFePO_4$ electrodes and analyzed the ablation depth of the resulting profiles with an optical profiler. Demir and Previtali (2014) compared the cut quality achieved with green lasers and

* Correspondence to: viale Risorgimento 2, 40136 Bologna, Italy.
E-mail address: erica.liverani2@unibo.it (E. Liverani).

https://doi.org/10.1016/j.jmatprotec.2023.118266
Received 14 July 2023; Received in revised form 8 November 2023; Accepted 15 December 2023
Available online 19 December 2023

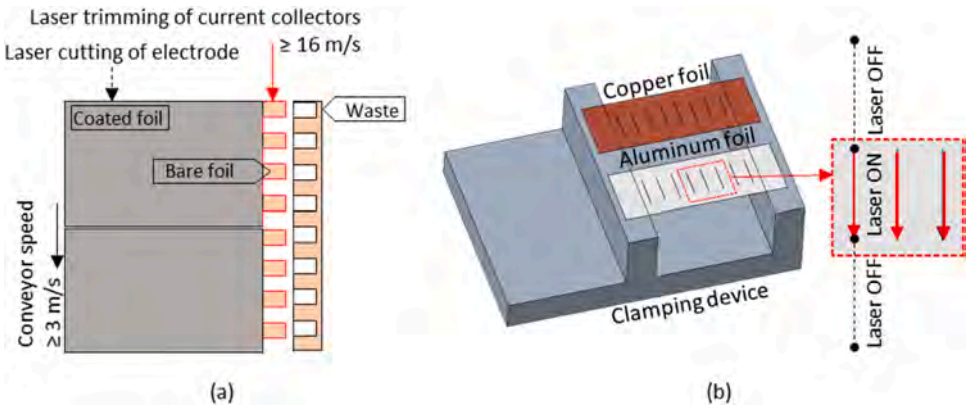

Fig. 1. Laser cutting (or trimming) path of current collectors (a) and experimental cutting setup (b).

infrared lasers, highlighting that with both solutions, pulsed lasers cause localized heating.

The size of the heat affected zone (HAZ) has a significant impact on the resulting cut quality of electrodes; therefore, several authors have addressed this aspect. Schmieder (2017) investigated the composition of the HAZ in relation to the pulse width, finding that the HAZ is substantially smaller than the actual deposition width of ablated material. Lutey et al. (2014) showed that chemical and microstructural alterations in electrode active layers are limited to the visible HAZ. Given the widespread use of pulsed lasers for electrode cutting, many studies have been conducted with this type of source. Nanosecond pulsed lasers are the most commonly cited; however shorter pulse durations have also been investigated to determine potential quality improvements. Zhang. et al. (2019) investigated the use of laser pulses of duration 250 fs – 10 ps at cutting speeds of less than 1 m/s, determining that the HAZ could not be avoided under these conditions. However, similar research on cut quality was also conducted by Baumann et al. (2019) using a continuous-wave (CW) single-mode fiber laser, with preliminary findings presented for cutting speeds of up to 10 m/s. Current collectors employ highly reflective and conductive materials, copper and aluminum, representing a significant challenge for electromobility, as illustrated by Mei et al. (2023) and Kim et al. (2022) for laser welding. However, industrial laser cutting of metallic foils is not currently done with CW green or blue lasers because of their larger focused spot size and lower beam quality when compared to CW IR lasers. On the other hand, new and interesting pulsed green lasers are currently on the market and show promise for this use, but they are expensive and have fixed duration. Luetke et al. (2011) investigated contact-free cutting of Cu and Al foils of thickness 6 and 12 μm, respectively, using two different laser sources to establish the cut quality. Both continuous-wave (CW) and nanosecond pulsed-wave (PW) lasers were exploited to determine the achievable cutting speed and quality in each case, with general fields of application described for both types of laser exposure. The cutting speed, however, was limited to less than 5 m/s in this case. To the best of the authors' knowledge, there have been no comparisons between CW and PW laser cutting of current collectors at speeds higher than 5 m/s. To meet the demands of the automotive industry, the output rates of gigafactories must be approximately one battery per second, requiring cutting speeds of at least 16 m/s. Motion systems that allow such high speeds are relatively new; therefore, the nature of laser-material interactions and the final cut quality at these speeds are currently key areas of research. Because current collectors are used to obtain an electrical connection with the battery cup after trimming and rolling of electrodes, detrimental defects are primarily associated with the edge profile. Wu at al. (2019) identified two types of hazards causing internal short circuits in Li metal batteries: 1) Physical contact between the cathode and anode due to material defects, manufacturing issues (like burrs, particles, and dust), and battery abuse conditions; 2) Contact resulting from chemical and/or electrochemical reactions. Jansen et al. (2019) linked these two factors to spatter formation. Uneven current distribution caused by spatter promotes dendrite growth across the separator, leading to micro-short circuits and early battery failure. For this reason, the main industrial requirement is to eliminate or reduce spatter as much as possible, as well as control dross formation. Dross is residual material that remains attached to the cut edge, developing as a result of insufficient vaporization of the material during the cutting process (Schulz et al., 1999). Furthermore, the kerf width must be minimized to lessen production waste during electrode cutting and trimming. Defect formation is significantly influenced by the melt pool and heat flow, as well as intensity and pressure distributions during laser cutting. Several research groups have sought to understand how these physical processes affect interaction between the laser and material. Lee (2018) described the physical mechanism of partial penetration of current collectors during laser cutting as a physical phenomenon leading to defects. Lee and Mazumder (2018) provided an interesting explanation of spatter formation, correlating this defect to the formation of a crest resulting from liquid metal flow during the cutting process. Molten material is moved from the bottom towards the sides of the keyhole, and then beyond the top surface of the foil by momentum, becoming spatter upon re-solidification. The resulting molten metal forms dross when it solidifies along the cut edge. All of these defects are strictly related to laser-material interaction phenomena and thus vary depending on the optical system and power delivery mode (PW or CW), making comparison of the two laser sources important.

The present paper therefore proposes a comprehensive comparison of CW and PW laser cutting of uncoated pure aluminum and copper current collectors, achieving industrially-relevant scanning speeds of up to 28 m/s for the first time. Results are focused on determining the effects of laser irradiance (the ratio of laser power to spot area) and fluence (the product of irradiance and interaction time) on defects that occur during remote ultra-high-speed laser cutting of aluminum and copper current collectors. Analyses with an Optical Microscope (OM) and Scanning Electron Microscope with Field Emission Gun Microscope (SEM/FEG-EDS) have been performed to characterize the cut quality and correlate these properties with the laser source and process parameters. Final results allow identification of an appropriate process parameter window for both materials and sources.

2. Materials and methods

2.1. Materials, laser sources and cutting setup

A simple metal foil geometry and linear cutting path were considered to characterize and optimize the laser trimming process used for current collectors (see Fig. 1). Strips of copper (CuAg ≥ 99.8%) and aluminium (1100 alloy, wt% Al ≥ 99.0%, Fe ≤ 0.5%, Si ≤ 0.5%, Cu ≤ 0.2% other

Table 1
Detailed characteristics of laser sources and optics.

CW	Maximum Power [kW]	1.2
	M^2	≤ 1.1
	Collimation length [mm]	120
	Focal length [mm]	340
	Fiber core diameter [μm]	14
	Spot diameter [μm]	65
	Wavelength [nm]	1064
PW	Average power [W]	300
	Max peak power [kW]	10
	Max pulse energy [mJ]	2
	Max repetition rate [kHz]	4000
	Pulsed duration [ns]	20-500
	M^2	1.5
	Collimated beam diameter [mm]	8
	Focal length [mm]	100
	Spot diameter [μm]	25
	Wavelength [nm]	1064

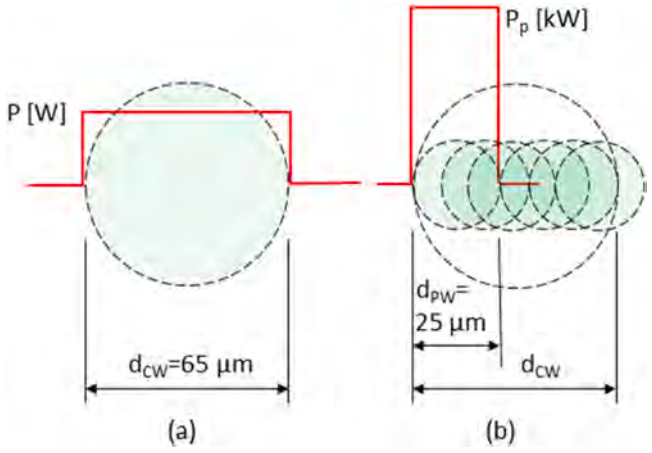

Fig. 2. Model for comparison of CW and PW lasers over the same circular area of diameter d_{CW}.

elements $\leq$ 0.05%) foil, 6 μm and 12 μm thick respectively, were cut from rolls and held under slight tension in a clamping system to keep the foils precisely positioned in the focal plane during cutting. Each strip was 20 mm × 60 mm in size, with parallel laser cuts performed over a length of 10 mm in each case. To avoid thermal interaction and local deviation of the material from the focal plane, the distance between subsequent cuts was 5 mm, while a maximum of 10 cuts were made on each strip. Laser systems employed for experiments included a continuous-wave (CW) nLight 1200 W single mode laser source (nLight, Washington, US) and a pulsed-wave (PW) IPG YLPN 300 W nanosecond ytterbium fiber laser (IPG Photonics Corporation, Massachusetts, US). These laser sources are currently the most promising for cutting current collectors because they have the power (or peak power with high frequency) to complete a cut at scanning speed up to 20 m/s. Furthermore, thanks to the high quality of the laser beam (see Table 1), very high cut quality is expected together with narrow kerf and low thermal dissipation. The CW system was equipped with a 14 μm core optical fiber for beam transportation and a Scanlab IntelliScan 20 galvanometric scanning head for beam movement, equipment with an f-theta lens with an effective focal length of 340 mm. The spot size was measured as 65 μm using a beam profiler (BeamWatch®, Ophir, Germany) in line with the standard measurement method set out in ISO 11146. For the PW system, beam movement was achieved with a Raylase Superscan II 10 equipped with an f-theta lens with a focal length of 100 mm, achieving a final spot size 25 μm.

To avoid heat accumulation within the current collectors, the laser cutting process was designed to account for galvo-mirror acceleration and deceleration, excluding these from the analysis (see Fig. 1b).

The laser beam was only turned on in the central part of the path, while the extension over which the laser beam was turned off was determined with a preliminary experimental campaign. As noted previously, both foils were held in the focal plane during all tests. Table 1 summarizes the complete characteristics of both setups.

2.2. Cutting parameters

In order to compare laser cutting under PW and CW conditions, the model for laser-material interaction displayed in Fig. 2 was adopted. Fig. 2a depicts the interaction of a CW laser beam with power P and spot diameter d_{CW}, while Fig. 2b depicts the interaction of a PW laser beam over the same area with peak power P_p and spot diameter d_{PW}.

Based on this model, the irradiance (I_{CW} and I_{PW}), fluence (F_{CW}) and equivalent fluence (F_{PW}) were calculated for PW and CW exposure in line with Eqs. 1–4.

$$I_{CW} = \frac{P}{A_{CW}} \quad \left[\frac{MW}{cm^2}\right] \tag{1}$$

$$I_{PW} = \frac{P_p}{A_{PW}} \left[\frac{MW}{cm^2}\right] \tag{2}$$

$$F_{CW} = I_{CW} \bullet \tau = I_{CW} \bullet \frac{d_{CW}}{Speed} \left[\frac{J}{cm^2}\right] \tag{3}$$

$$F_{PW} = F_{PW,p} \bullet N_p = I_{PW} \bullet t \bullet N_p = I_{PW} \bullet \tau_{EQ} \left[\frac{J}{cm^2}\right] \tag{4}$$

where A_{CW} and A_{PW} are the spot areas of the CW and PW laser beams

Table 2
Process parameters employed for CW laser cutting tests.

	P [W]	I_{CW} [MW/cm2]	Laser speed [m/s]	F_{CW} [J/cm^2]		P [W]	I_{CW} [MW/cm^2]	Laser speed [m/s]	F_{CW} [J/cm^2]
CW_A1	170	5.1	4.75	70	CW_C4	660	19.9	5.2	250
CW_A2	330	9.9	9.2		CW_C5	830	25.0	6.5	
CW_A3	500	15.1	14		CW_C6	1000	30.2	7.8	
CW_A4	660	19.9	18.5		CW_D1	170	5.1	0.95	350
CW_A5	830	25.0	23		CW_D2	330	9.9	1.85	
CW_A6	1000	30.2	28		CW_D3	500	15.1	2.8	
CW_B1	170	5.1	2.8	120	CW_D4	660	19.9	3.7	
CW_B2	330	9.9	5.4		CW_D5	830	25.0	4.6	
CW_B3	500	15.1	8.2		CW_D6	1000	30.2	5.6	
CW_B4	660	19.9	10.7		CW_E1	170	5.1	0.65	500
CW_B5	830	25.0	13.5		CW_E2	330	9.9	1.3	
CW_B6	1000	30.2	16.3		CW_E3	500	15.1	1.95	
CW_C1	170	5.1	1.35	250	CW_E4	660	19.9	2.6	
CW_C2	330	9.9	2.6		CW_E5	830	25.0	3.2	
CW_C3	500	15.1	3.9		CW_E6	1000	30.2	3.9	

Table 3
Process parameters employed for PW laser cutting tests.

	E_p [mJ]	Pulse duration [ns]	P_p [kW]	f [kHz]	I_{PW} [MW/cm^2]	Laser speed [m/s]	N_p	F_{PW} [J/cm^2]
PW_A1	0.3	240	1.3	1000	255	20.7	3.14	192.0
PW_A2	0.2	120	1.7	1500	340	20.7	4.71	
PW_A3	0.1	20	5.0	3000	1019	20.7	9.42	
PW_A4	0.15	20	7.5	2000	1529	20.7	6.28	
PW_A5	0.5	60	8.3	600	1699	20.7	1.88	
PW_B1	0.3	240	1.3	1000	255	16	4.06	248.4
PW_B2	0.2	120	1.7	1500	340	16	6.09	
PW_B3	0.1	20	5.0	3000	1019	16	12.19	
PW_B4	0.15	20	7.5	2000	1529	16	8.13	
PW_B5	0.5	60	8.3	600	1699	16	2.44	
PW_C1	0.3	240	1.3	1000	255	8	8.13	496.8
PW_C2	0.2	120	1.7	1500	340	8	12.19	
PW_C3	0.3	240	1.3	1000	255	8	8.13	
PW_C4	0.15	20	7.5	2000	1529	8	16.25	
PW_C5	0.5	60	8.3	600	1699	8	4.88	
PW_D1	0.3	240	1.3	1000	255	4	16.25	993.6
PW_D2	0.2	120	1.7	1500	340	4	24.38	
PW_D3	0.1	20	5.0	3000	1019	4	48.75	
PW_D4	0.15	20	7.5	2000	1529	4	32.50	
PW_D5	0.5	60	8.3	600	1699	4	9.75	

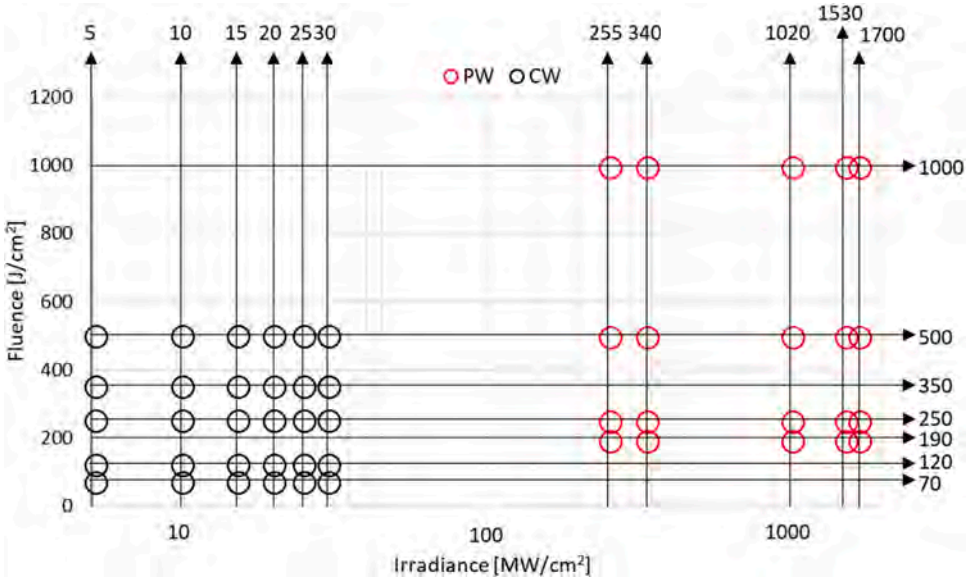

Fig. 3. Summary of laser cutting experimental campaign for PW (red dots) and CW (black dots) laser sources.

considering respective spot diameters of 65 μm and 25 μm, τ is the interaction time for CW exposure, $F_{PW,p}$ is the pulse fluence for PW exposure, and t is the pulse duration. For the purposes of comparing fluence, the number of pulses (N_p) generated by the PW laser was calculated based on Eq. 5, allowing definition of the equivalent interaction time (τ_{EQ}) based on Eq. 6.

$$N_p = \frac{d_{CW} \bullet f}{Speed} \tag{5}$$

$$\tau_{EQ} = t \bullet N_p \tag{6}$$

Detailed process parameters are reported in Tables 2 and 3 for tests conducted with the CW and PW laser sources, respectively. For CW experiments, a total of 5 fluence levels and 6 irradiance levels were employed. Due to limitations in combining process parameters for PW experiments, 4 equivalent fluence levels and 5 irradiance levels were evaluated for this type of exposure.

Two fluence levels (250 and 500 J/cm^2) coincided between the two laser sources; however, no corresponding values of irradiance could be established due to the high peak power of the PW laser source (see Fig. 3). Final process parameters were established based on the outcomes of preliminary tests, which are not the focus of this paper, with the intention of examining all physical phenomena related to laser cutting of thin films at high processing speeds.

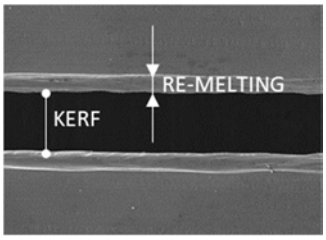

Fig. 4. Definition of kerf width and re-melting thickness.

2.3. Characterization of cut quality

Optical microscopy (OM, Nikon Optiphot-100) was performed to a

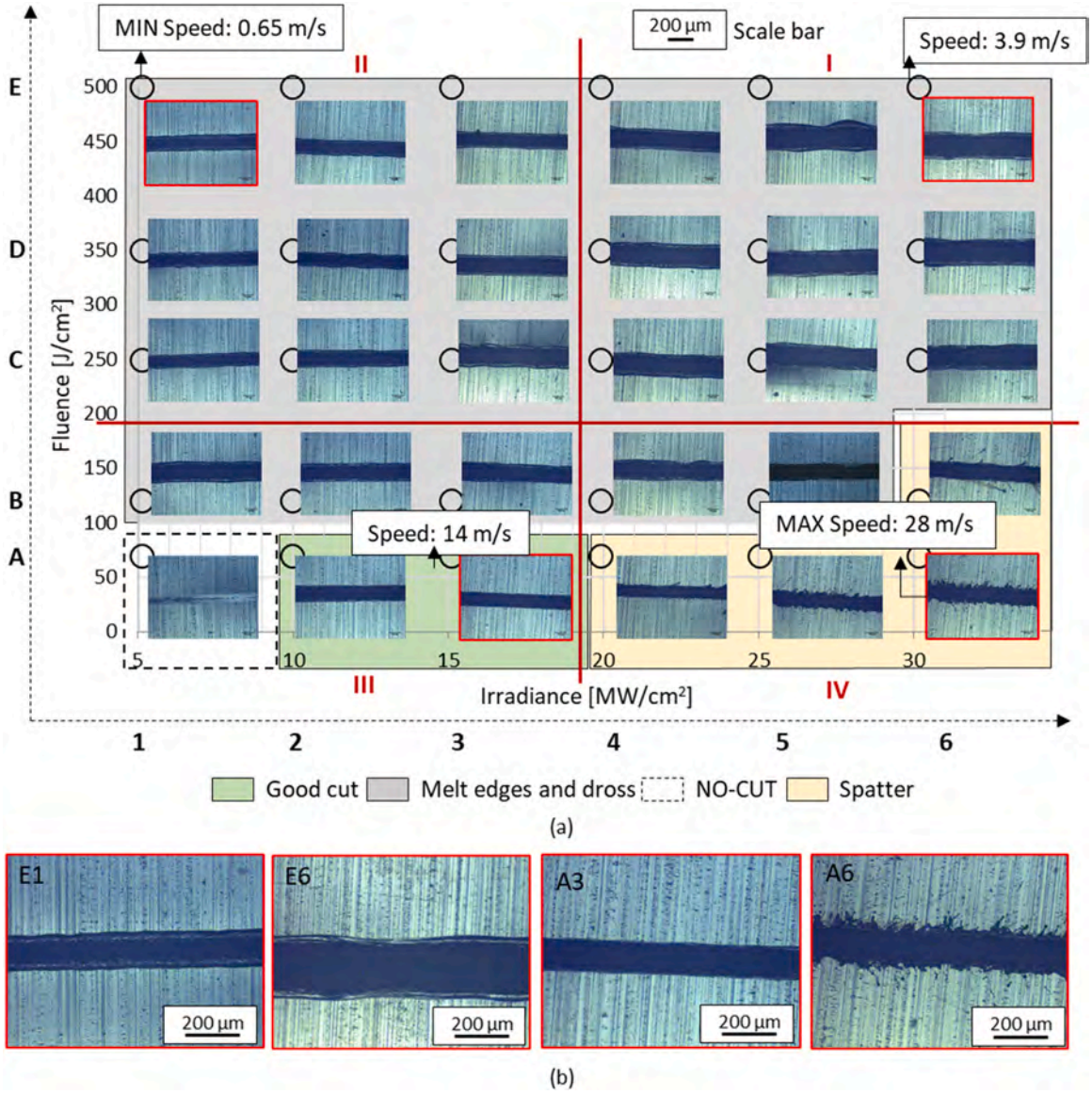

Fig. 5. OM images of CW laser cuts performed on aluminum current collectors (a) and enlargement of representative cuts (b) performed with the following process parameters: 170 W and 0.65 m/s (E1), 1000 W and 3.9 m/s (E6), 500 W and 14 m/s (A3), 1000 W and 28 m/s (A6).

provide preliminary assessment of cut quality and identify general defects for each combination of process parameters in terms of uncompleted cuts, spatter, burns, melted edges, dross, and presence of a HAZ. Furthermore, the kerf width was determined for all tests (see Fig. 4), with the mean value calculated based on 3–5 data points collected along the entire cut. SEM-FEG microscopy (Tescan Mira3 with a Schottky emitter) was then used to examine representative cuts on both the front surface (the area directly subject to laser irradiation) and the underside of each foil. Each cut was observed via SEM at the start, middle, and end of the laser path.

3. Results

3.1. Continuous-wave laser cutting

Representative images of different cut morphologies obtained on aluminum current collectors with CW laser exposure are reported in Fig. 5, considering irradiance as the driving input parameter for the various experiments. Cutting geometries were initially divided into "good cut" and "bad cut" categories, with the latter being further divided based on the primary type of defect in each case. Bad cuts were catalogued as “over-melted” when the thickness of resolidified metal was greater than 25% of the kerf width, and “sputter-cut” when the presence of sputtering was predominant (see Fig. 6). With an irradiance level of less than or equal to 5 MW/cm^2 and a fluence level of less than 100 J/cm^2, the current collectors remained uncut or partially uncut, as seen in Fig. 5a. Fluence levels greater than 100 J/cm^2 led to over-melted edges at all levels of irradiance. This region of high fluence combined with low irradiance (II quadrant) led to melted edges and dross formation (the gray area in Fig. 5a) characterized by different levels of over-melting that were considered critical or unacceptable (re-melting/kerf width ratio from 25% to 65%). The ratio of melted edge thickness to kerf width decreased from quadrant II to all other quadrants (see Fig. 4), with higher values of both parameters observed in quadrant I (high fluence and high irradiance). Finally, spatter was observed at high levels of irradiance and low fluence (IV quadrant). After identifying the regions where the main defects were located, it was clear that the best combination for achieving good cut quality was low fluence and low irradiance.

The samples highlighted by red frames (enlarged in Fig. 5b) were

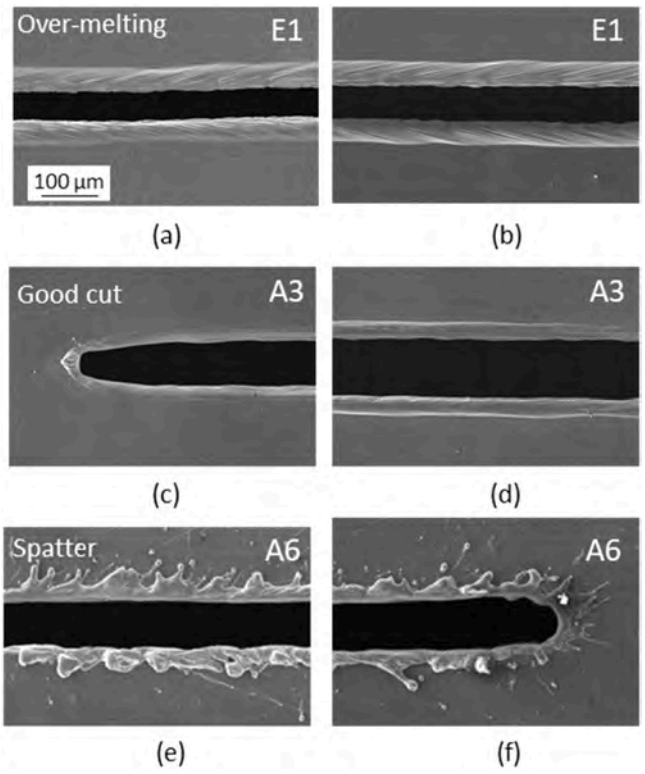

Fig. 6. SEM images (SE, 10 kV) of CW laser cuts performed on aluminum current collectors: (a,b) cut with over-melted edge (170 W, 0.65 m/s), (c,d) good cut (500 W, 14 m/s) and (e,f) spattered cut (1000 W, 28 m/s).

chosen for SEM analysis (Fig. 6) as representative of cut quality obtained in each process region. The selected cut in quadrant I was characterized by a larger kerf, that in quadrant II by a severely over-melted edge, that in quadrant III by high cut quality and that in quadrant IV by spatter. Parts a and b of Fig. 6 display the front and back sides of the cut obtained with parameter set CW_E1 (see Table 2). It is worth noting that the over-melted edges were very homogeneous on both sides, which was observed along the entire cut. No dross formation was found on aluminum current collectors using this parameter set or any other parameters employed during CW laser irradiation.

Parts a and b of Fig. 6 highlight the fact that a large quantity of molten material is not ejected from the bottom of the current collector but remains adherent to both the top and bottom surfaces. A ridge can be seen along the cut edge, with the width depending on the specific process parameters employed. In the case of CW_E1, the mean ridge width was 40 µm in the middle of the cut, while the kerf was 48 µm, yielding a ratio of 0.83. Very similar cut quality was identified for other samples within quadrant I (CW_E6). The respective images are not reported as the kerf increased to 215 µm, with the ratio between the ridge and kerf widths decreasing to 0.29. The same considerations can be made for high quality cuts (Fig. 6c and d, sample CW_A3); however, in this case, the size of the kerf and remelted width are significantly smaller, 160 µm and 45 µm respectively, with the same ratio of 0.28. By observing the final part of the cut in Fig. 6c, the melted metal generates an appendage on the cut edge, with the same phenomenon visible on the underside in the initial part of the cut. For completeness, this defect was analyzed on cuts performed with parameters similar to CW_A3, with the defect present in all cases; however, the molten droplet was identified on both surfaces without a direct correlation with the position of the start and end of the cut. It was sometimes found on the front surface at the start of the cut and other times at the end of the cut and vice versa. Images of the spattered sample (CW_A6) are shown in Fig. 6e and f. Due to melt turbulence, the profile of the melted edges was no longer uniform, with spatter ejected far from the laser path onto the surface around the cut in the middle (e) and partially at both ends (f), over a width of 250–300 µm.

Representative images of different cut morphologies obtained on copper current collectors with CW laser exposure are reported in Fig. 7.

With reference to Fig. 7a, a larger number of parameters led to no cut or a partially cut than was observed for aluminum over the same irradiance and fluence ranges. Despite the copper current collector being thinner, this result was in line with expectations due to lower optical absorptivity of copper in the near infrared. To achieve a complete cut with fluence below 100 J/cm^2, it was necessary to employ an irradiance level greater than 25 MW/cm^2. As with aluminum, high-quality cuts were achieved with process parameters near the uncut region.

It is immediately clear from Fig. 7a that copper exhibited a wider parameter range leading to high quality cuts than aluminum, suggesting a better response of copper to ultra-high-speed laser cutting. The wider range of parameters leading to good quality was due to lower levels of spattering, with defects confined to speeds greater than 25 m/s, at the operating limit of current galvanometric scanning heads. Melted edges were obtained over a similar range of process parameters to aluminum but with two important differences in relation to edge melting and the presence of burns. Edge melting was not homogeneous but was localized to very small areas, with melted droplets appearing at relatively regular intervals depending on the specific parameters employed, and dross formation resulting from localized heat accumulation rather than as a continuous ridge. Burning instead affected a broad range of parameters in quadrant I, overlapping with regions within quadrants I and II where defects relating to melting were also observed. Despite burns being more evident at higher fluences, this defect was relatively limited and only affected a relatively limited area of the surfaces under all process conditions. The samples highlighted by red frames (enlarged in Fig. 7b) were chosen for SEM analysis (Fig. 8) as representative of cut quality in each process region. Fig. 8a and b display SEM images of samples located in quadrant I (CW_E6) and quadrant II (CW_E1), respectively, both of which were affected by edge melting. The appearance of the former was similar to that observed for aluminum under the same process conditions but with some width irregularities, while the latter was characterized by melting in the form of dross, as was observed with all combinations of process parameters employing high fluence and medium or low irradiance. In both cases, no relevant difference in cut quality was observed between the front and back sides. Conversely, process parameters leading to high cut quality (B4 in Fig. 8c and d) led to a significant difference between the characteristics of the two sides. The upper side, on which laser interaction took place, was free of melting, which was instead visible on the underside in the form of a narrow homogeneous ridge similar to that observed for aluminum, with the ratio between the melt width (30 µm) and kerf (135 µm) being 0.22. Due to the formation of less molten material along the edges, the spattered sample (A6, Fig. 8e and f) also exhibited a lower quantity of ejected material. However, copper spatters reached a distance from the laser path similar to that of aluminum, with molten droplets affecting both the upper and lower surfaces of the current collector (Fig. 8c and d).

3.2. *Pulsed-wave laser cutting*

Significant differences in cut quality were observed when switching to PW laser cutting. Despite the same types of defects being observed, the impact of these defects on the quality of the resulting cuts was more evident, in particular on aluminum samples. Fig. 9 displays images of the cut quality obtained on aluminum current collectors with the parameters given in Table 3. As observed for CW cutting, high fluence caused over-melted edges at all levels of irradiance. However, the over-melting threshold increased for PW cutting, rising to above 250–500 J/cm^2. In addition, melted edges were irregular, with this discontinuity worsening as irradiance increased despite the fact that the melted region was narrower.

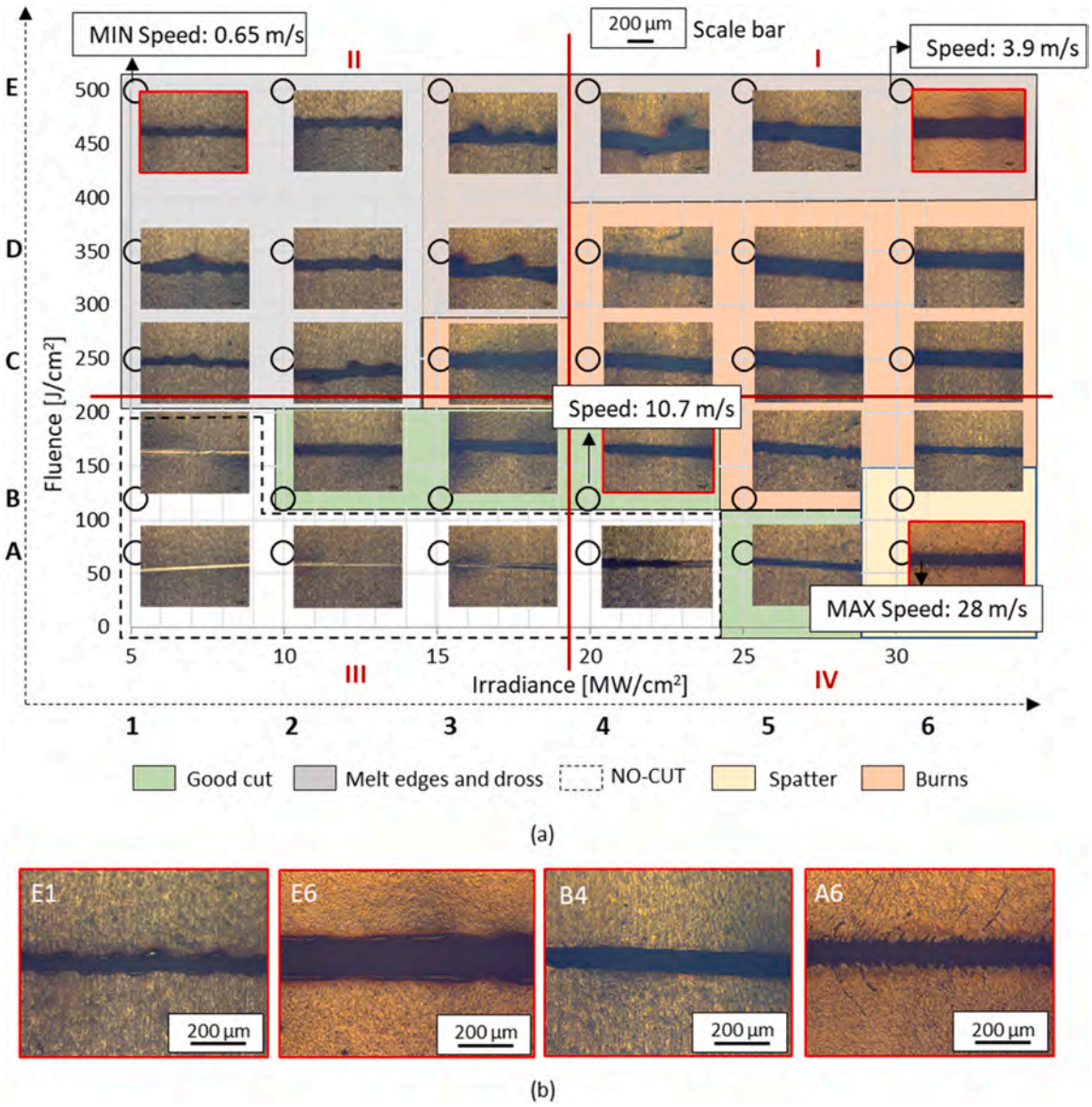

Fig. 7. OM images of CW laser cuts performed on copper current collector (a) and enlargement of representative cuts (b) performed with the following process parameters: 170 W and 0.65 m/s (E1), 1000 W and 3.9 m/s (E6), 660 W and 10.7 m/s (B4), 1000 W and 28 m/s (A6).

At the opposite end of the tested parameter window, where low fluence levels were employed, spatter and burns were instead the main types of defects observed. The latter appeared as dark regions adjacent to the cut edges, with the effect being more pronounced at higher irradiance levels. Best cut quality was obtained at a cutting speed of 16 m/s at all irradiance levels; however, upon comparison of the best cuts obtained with PW (Fig. 10c) and CW (see Fig. 8c) laser sources, worse cut quality was evident in the former case.

Following the same criteria for selection of samples for SEM analysis, representative images of the obtained cut quality in each process region are shown in Fig. 10, including samples exhibiting melting (PW_D2), burning (PW_C5), high cut quality (PW_B2) and spattering (PW_A4). No underside images are provided as these surfaces exhibited the same characteristics as the top sides. Comparison of OM and SEM images leads to the following observations:

- While edge remelting (Fig. 10a) was not as homogeneous as with CW laser cutting, this type of defect was nonetheless similar under both CW and PW conditions. Despite the smaller spot diameter employed in the PW setup, the kerf width of sample PW_D2 was comparable with that of sample CW_E1 due to twice the fluence being employed.
- The highest cut quality achieved with the PW laser (Fig. 10c) was not completely free of small, rounded droplets of material within the entire region surrounding the cut due to turbulence of the molten phase during laser exposure.
- Spatter (Fig. 10d) was abundant but more contained around the cut, up to 130 µm from the center of the cut.
- No burns were visible in SEM images, confirming that no state changes were associated with this defect.

Fig. 11 displays images of the cut quality obtained on copper current collectors with the PW laser setup. The same general considerations can be made as for aluminum in terms of defect formation. In this case, process parameters leading to good cut quality were those employing low irradiance levels, while a wider range of parameters comprising high irradiance led to the development of burns.

Finally, edge melting was less of an issue for copper, as was observed for CW cutting, suggesting that differences in this aspect were due to material properties rather than the type of laser exposure.

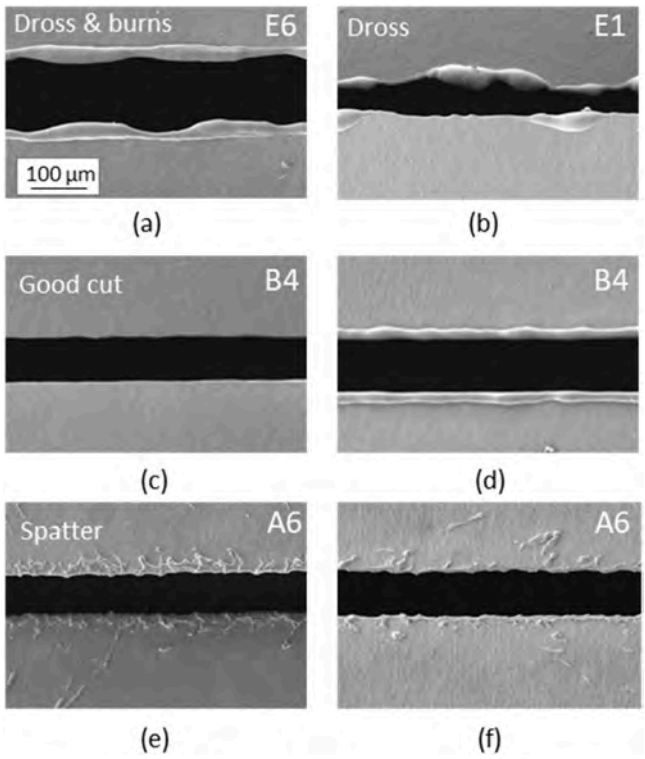

Fig. 8. SEM images (SE, 10 kV) of CW laser cuts performed on copper current collectors: (a,b) cut with dross (1000 W, 3.9 m/s) and burns (170 W, 0.65 m/s), (c,d) good cut (660 W, 10.7 m/s) and (e,f) spattered cut (1000 W and 28 m/s).

3.3. Kerf width measurements

The results of kerf width measurements were analyzed based on three levels of comparison. The first (Level 1) compared the influence of the *laser source* on the kerf width, the second (Level 2) the influence of the *material* and the third (Level 3) the influence of the *process parameters* in terms of fluence and irradiance.

The Level 1 comparison (influence of laser source) was performed by calculating the mean width and standard deviation of all cuts obtained with both laser sources. The resulting values were 36 ± 14 µm for the PW laser source and 90 ± 5.5 µm for the CW source. The Level 2 comparison (influence of material) was performed by calculating the mean width obtained using PW and CW sources for both materials. The results of this comparison are presented in Table 4.

Finally, the Level 3 comparison (influence of process parameters) was performed by calculating the mean kerf width obtained under all conditions having constant values of fluence or irradiation for each combination of laser source and material. For example, the value represented by the first bar on the left of Fig. 12a (highlighted by a single red asterisk) was obtained by averaging the measured kerf widths of samples CW_A1, CW_A2, …, CW_A6, which all employed the same fluence level of 70 J/cm^2. In the same way, the value represented by the second bar (highlighted by two red asterisks) was obtained by averaging the measured kerf widths of samples CW_B1, CW_B2, …, CW_B6. An analogous comparison in terms of irradiance is presented in Fig. 12b. The value represented by the first bar (highlighted by a single black asterisk) was obtained by averaging the measured kerf widths of samples CW_A1, CW_B1, …, CW_E1, and so on.

4. Discussion

One of the main goals of battery production is to achieve high productivity and quality, conditions that directly apply to cutting of battery current collectors. To date, a comprehensive study of feasible laser sources, optics and process parameters has yet to be presented in the literature. As a result, a thorough investigation of CW and PW laser cutting of copper and aluminum current collectors was conducted within this work. In the following section, a detailed analysis of correlations between cut quality and material, power delivery, and process parameters is presented.

4.1. Correlation between cut quality and material

By employing the same process parameters for cutting of aluminum and copper current collectors, it was possible to demonstrate that aluminum required lower levels of irradiance and fluence despite being twice as thick. This behavior was connected to the material properties of the current collectors. During laser cutting of copper, material removal took place at lower rates than for aluminum due to copper's lower mean optical absorptivity and higher thermal conductivity. Once cutting was achieved, by comparing Figs. 5 to 11, it is interesting to note the more widespread presence of burns for copper than aluminum. While aluminum was only susceptible to burns at the highest tested value of irradiance (> 1000 MW/cm^2), copper current collectors had burnt edges at low irradiance (CW mode), although this effect was more confined. By observing Figs. 9 and 11, it is possible to infer that during cutting of aluminum current collectors, highest temperatures were confined to the kerf and a very limited area in the neighboring region. This outcome was due to the physical characteristics of the materials in question, considering that the thermal conductivity of aluminum at room temperature is almost half that of copper (210 W/mK vs. 395 W/mK). However, the absence of burns was replaced by a melted edge, which was always visible along the aluminum cut edge. According to Babadjanov et al. (2023), this demonstrates that materials with high thermal conductivity melt less and burn more due to faster heat dissipation, while materials with lower thermal conductivity exhibit melted edges as a result of localized heat accumulation. Additionally, when observing CW cuts, the remelted edge was typically uniform in width and shape for aluminum but irregular for copper due to discontinuous heat accumulation (see Fig. 7), in accordance with Lee et al. (2012).

From a broader perspective, it is possible to argue that the resulting cut quality of copper depended on both irradiance and fluence (Figs. 6–10), while that of aluminum depended more on the interaction time (i.e. fluence) than on power (i.e. irradiance). In fact, by comparing results obtained for aluminum at the same fluence level, the presence of specific types of defects or good cut quality occurred at all irradiance levels, in particular for PW laser cutting.

4.2. Correlation between cut quality and process parameters

Fig. 13 provides a summary of results presented previously to assist in interpreting the correlation between process parameters and cut quality.

Four types of defects were detected, with the following correlations between defect type and irradiance and fluence levels:

1. Predominance of remelted edge at high fluence and low irradiance
2. Spatter at low fluence
3. Burns at high irradiance
4. Incomplete cutting at low fluence and low irradiance

Good cut quality was achieved with moderate fluence levels and moderate-to-low irradiance levels. High irradiance levels led to the formation of a large amount of liquid phase due to high power, resulting in two main issues: a large kerf and spatter. In particular, where high power was combined with low speed, the resulting kerf width was very large due to the larger area over which thermal conduction led the material to reach its vaporization temperature. In contrast, where high irradiance levels were connected with fast speeds, the interaction time was short and the vaporization temperature was attained over a width

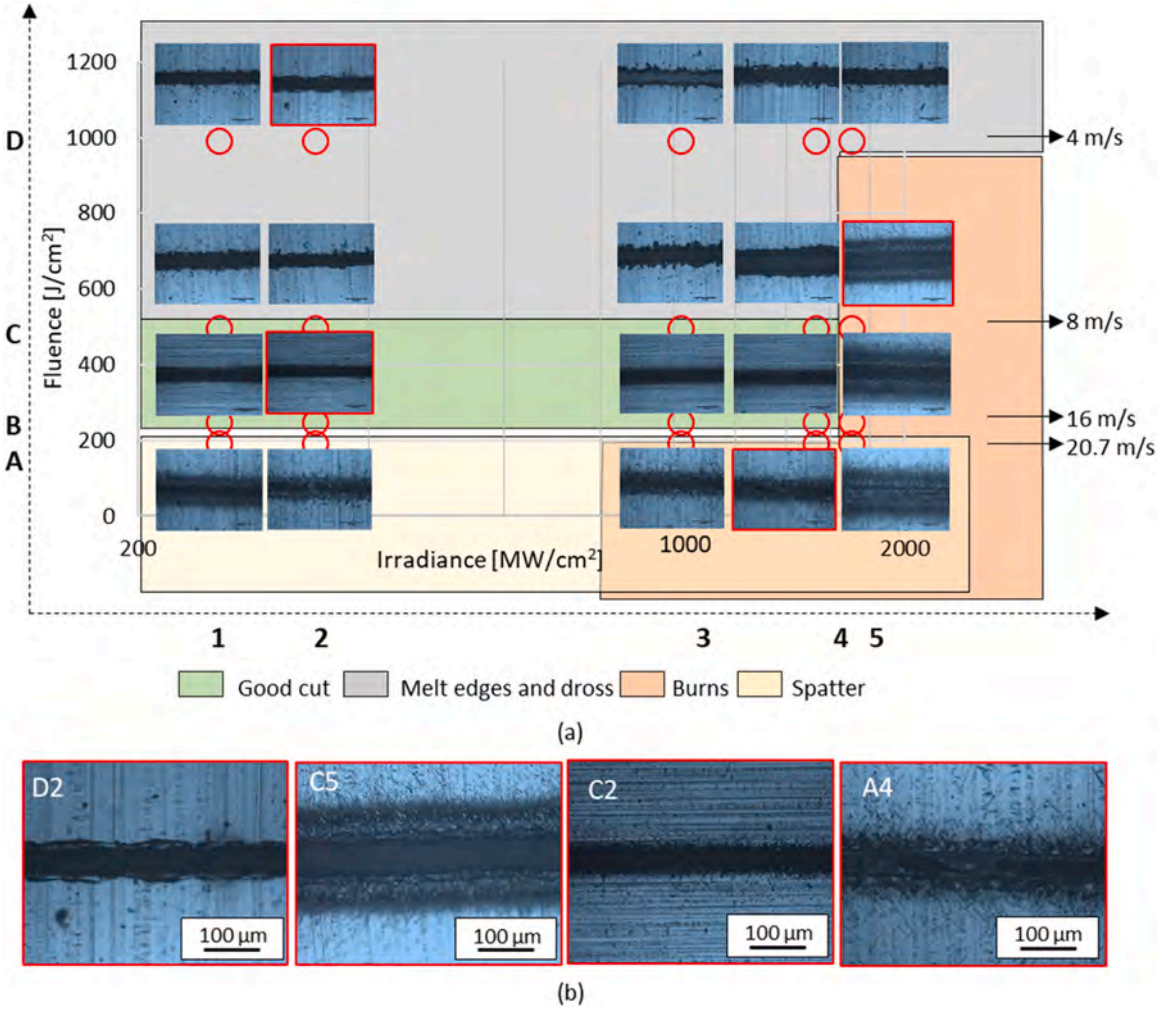

Fig. 9. OM images of PW laser cuts performed on aluminum current collector (a) and enlargement of representative cuts (b) performed with the following process parameters: 1.7 kW and 4 m/s (D2), 8.3 kW and 8 m/s (C5), 1.7 kW and 8 m/s (C2), 7.5 kW and 20.7 m/s (A4).

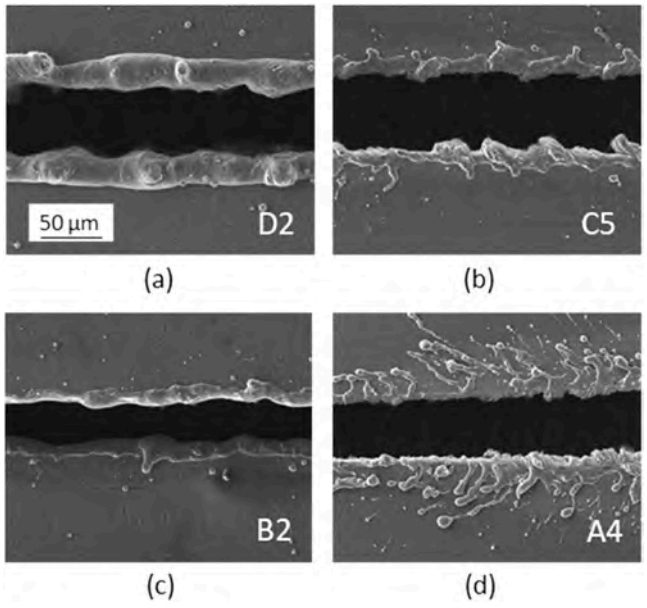

Fig. 10. SEM analysis (SE, 10 kV) of PW laser cuts performed on aluminum current collectors: (a) PW_D2, (b) PW_C5, (c) PW_B2 and (d) PW_A4 samples are shown.

that was smaller than the spot diameter, with melting of the cut edges. However, the high speed led to turbulence in the molten material, which in turn promoted spatter. For a given power, higher speeds nonetheless provided the best cutting conditions up until the onset of spatter.

Upon observation of the relationship between the cut quality of aluminum and the employed process parameters, a dependence on fluence becomes evident. Fig. 14a presents an image of a cut performed with the highest fluence, and consequently the longest interaction time, while Fig. 14b presents an image of a cut obtained with the highest irradiance and roughly half the fluence. SEM analysis shows that in the first case (PW_D2), a small kerf developed with a large extension of the heat affected zone (the white area), while in the second case (PW_C5), a large kerf developed but with a smaller HAZ. These outcomes can be explained in terms of the total heat input and peak temperature. The larger HAZ in the first case can be attributed to the larger heat input (i.e. longer interaction time), while the smaller kerf can be attributed to the lower peak temperature of D2 compared to C5 (i.e. lower peak power).

4.3. Correlation between cut quality and laser source

Although the current state-of-the-art for cutting of copper and aluminum current collectors (with or without coatings) is evolving from mechanical to pulsed laser cutting, the outcomes of this study demonstrate that the best quality is undoubtedly obtained with CW single mode lasers. Comparison of the two types of lasers requires complex assessment of laser-material interactions leading to the physical outcomes. It is

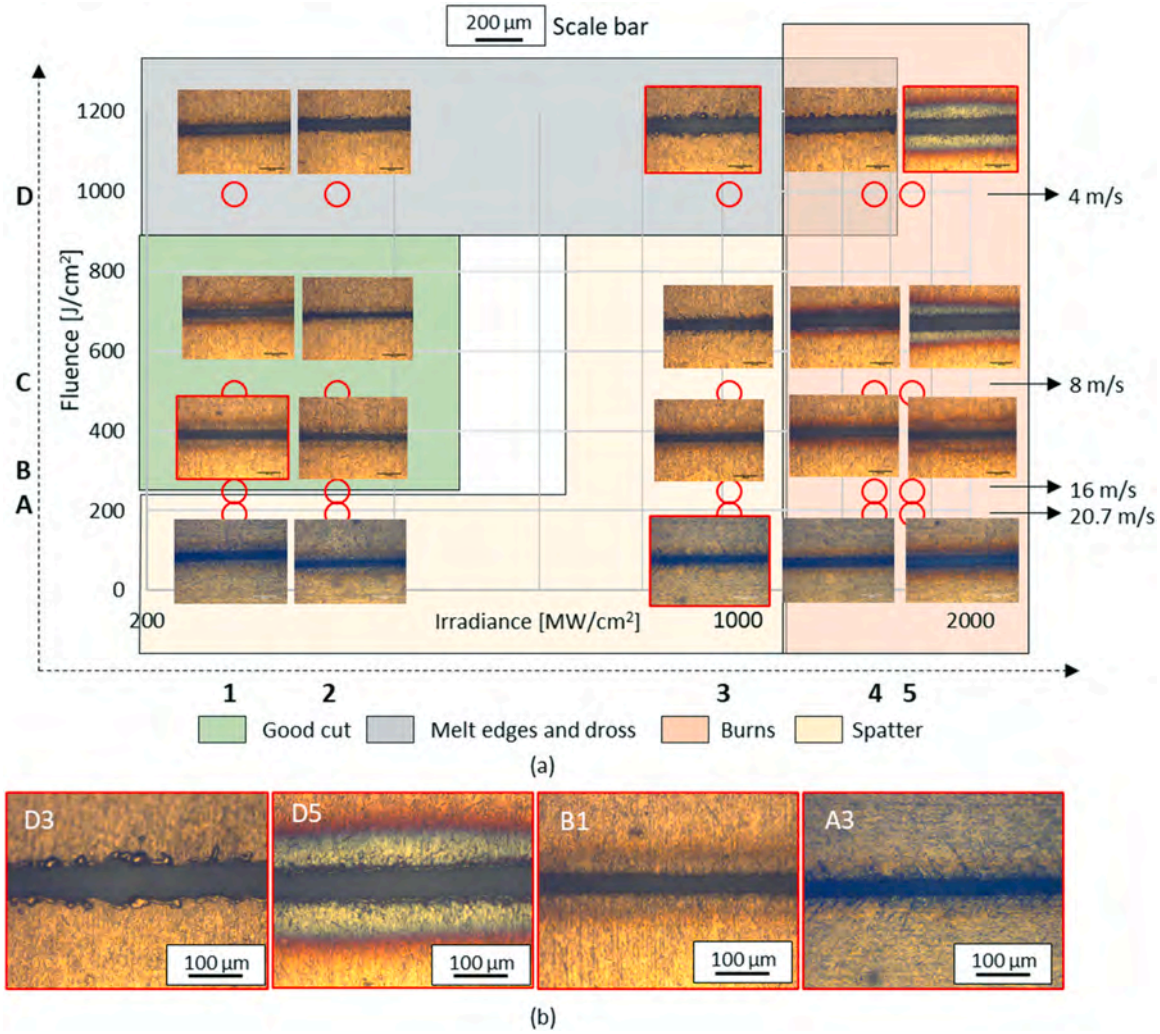

Fig. 11. OM images of PW laser cuts performed on copper current collectors (a) and enlargement of representative cuts (b) performed with the following process parameters: 5 kW and 4 m/s (D3), 8.3 kW and 4 m/s (D5), 1.3 kW and 16 m/s (B1), 5 kW and 20.7 m/s (A3).

Table 4
Influence of material (Level 2 comparison).

	ALUMINUM			COPPER		
	Mean [µm]	Std.Dev [µm]	Std.Dev/ Mean	Mean [µm]	Std.Dev [µm]	Std.Dev/ Mean
CW	**96**	23.8	0.25	**84**	28.9	0.34
PW	**35**	13.0	0.37	**36**	8.5	0.24

interesting to note that for CW laser sources, ideal cutting conditions were close to those leading to no cut, taking place at the highest tested cutting speed that could be achieved. This is consistent with literature in the field of laser cutting of sheet metal performed at lower cutting speeds (Wandera et al., 2009). The same consideration cannot be made for PW laser sources, where ideal cutting conditions were within a more central part of the process parameter window. The effect of vapor pressure in the pulsed regime goes beyond simple evaluation of phase changes (vaporization and melting) and heating by conduction. The explosive effect of vapor pressure on the molten phase requires optimization of cutting speed to be balanced with the prevention of dross at low speeds and spatter at high speeds. The final cutting quality was negatively affected by the contribution of vapor pressure across all parameters. Figs. 6 and 7 show that by using a CW source rather than a PW source, better results were obtained under all conditions, both optimal and suboptimal.

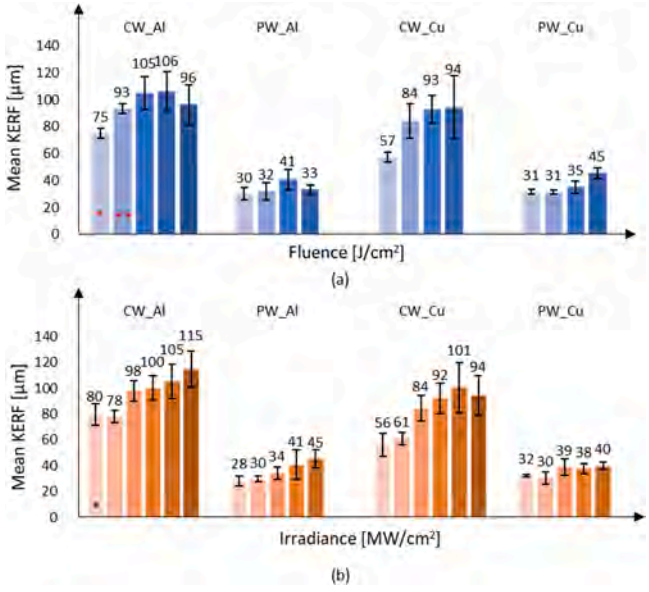

Fig. 12. Correlation between kerf width and fluence (a) or irradiance (b).

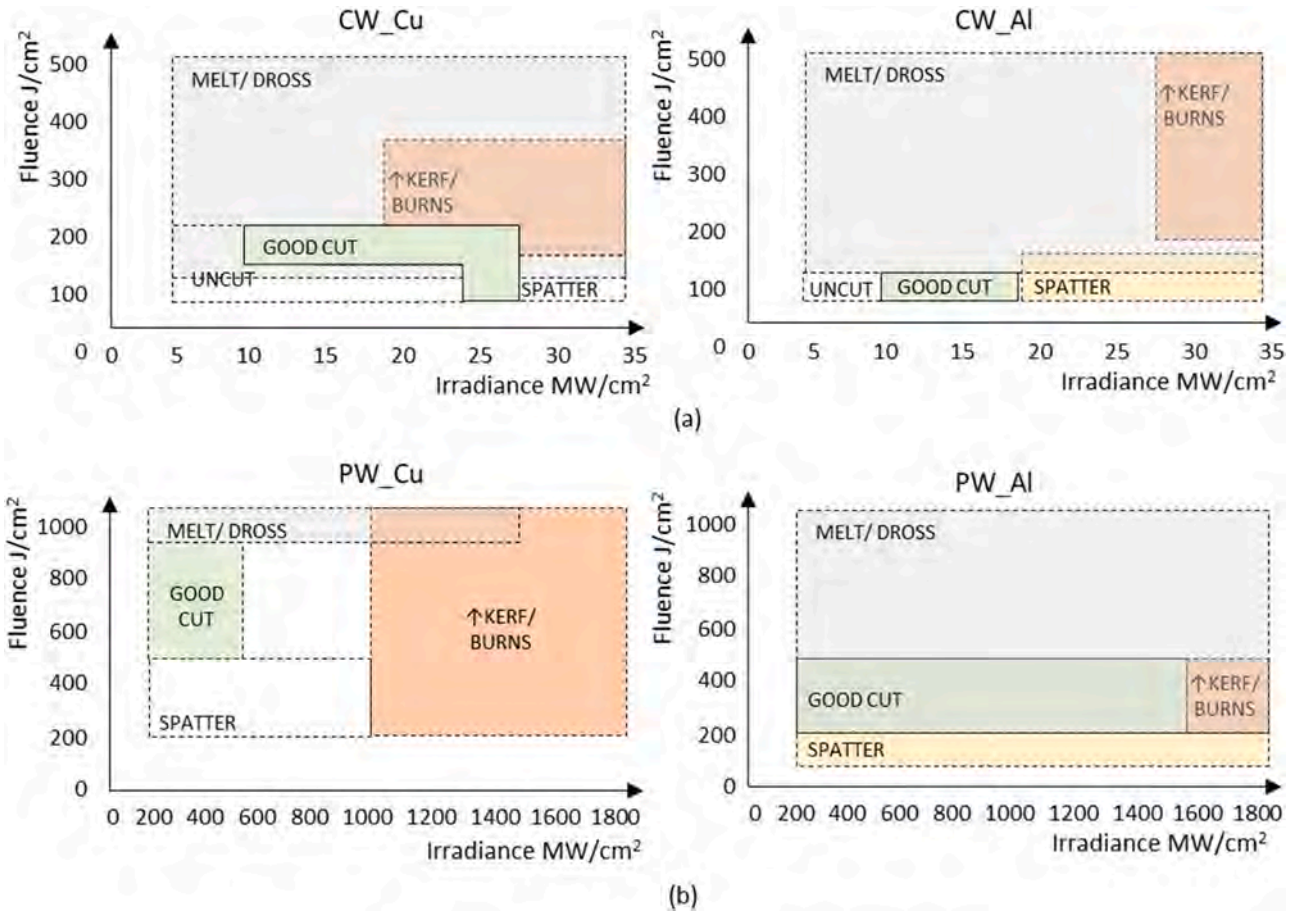

Fig. 13. Correlation between cutting parameters and defects for CW (a) and PW (b) laser sources.

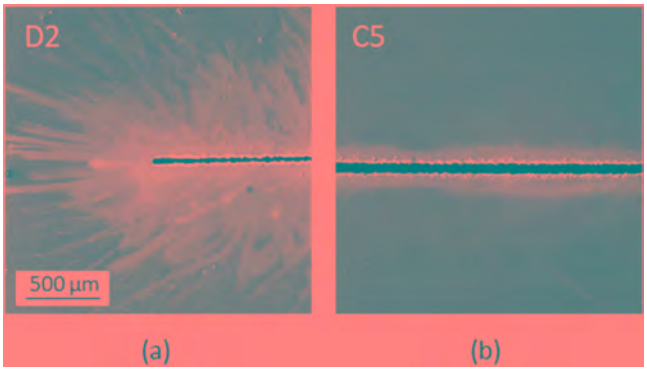

Fig. 14. Low magnification images of aluminum (a) PW_D2 (1.7 kW and 4 m/s) and (b) PW_C5 (8.3 kW and 8 m/s) samples.

4.4. Kerf width

The kerf width was generally highest in quadrant I, corresponding to high fluence and irradiance, as shown in Figs. 5, 7, 9, and 11. However, by examining the data provided in Section 3.3, more specific considerations can be made for each process variable.

Firstly, the result shows that the average kerf width obtained with the PW setup with a spot diameter of 25 µm was smaller than that obtained with the CW setup with a spot diameter of 65 µm. By comparing average values, the mean kerf width obtained with the PW source was 39.7% of that obtained with the CW source, with this value almost equal to the ratio of the two spot diameters (38.5%). This implies that the focusing system had a direct impact on the relationship between kerf width and laser setup. However, upon analysis of the standard deviation, it becomes clear that other variables such as the material and process parameters also influenced the kerf width. A value of 31% was obtained by dividing the standard deviation by the average value for both sources, proving once more that variability of the kerf width was linked to other parameters, with similar correlations for both PW and CW sources.

The effects of the most important process parameters on the kerf width were assessed by comparing data for the two tested materials. The average kerf width for copper was 88% of that obtained for aluminum with the CW laser source, while similar values were obtained for both materials with the PW laser source. As a result, the material had no effect on the obtained outcomes with the PW laser source and a moderate-to-low impact on outcomes obtained with the CW laser source. However, some additional considerations can be made by again focusing on the standard deviation.

For copper foils subject to CW laser exposure and aluminum foils subject to PW laser exposure, the ratio of the standard deviation to the mean value was higher, suggesting greater dependence on the specific process parameters employed and implying that process optimization is more difficult under these conditions. This outcome supports earlier conclusions relating to cut quality, including comparison of CW cutting results in Figs. 5 and 7. In fact, aluminum foils are typically cut with knife slitting or die cutting due to the challenging process of tuning laser parameters, whereas pulsed lasers are currently widely used for cutting of copper foils.

However, values of standard deviation in Table 4 suggest dependence of the kerf width on process parameters for all of the tested setups. As a result, further analysis of data in Fig. 12 is necessary. In order to better analyze the data presented for each comparison group, linear

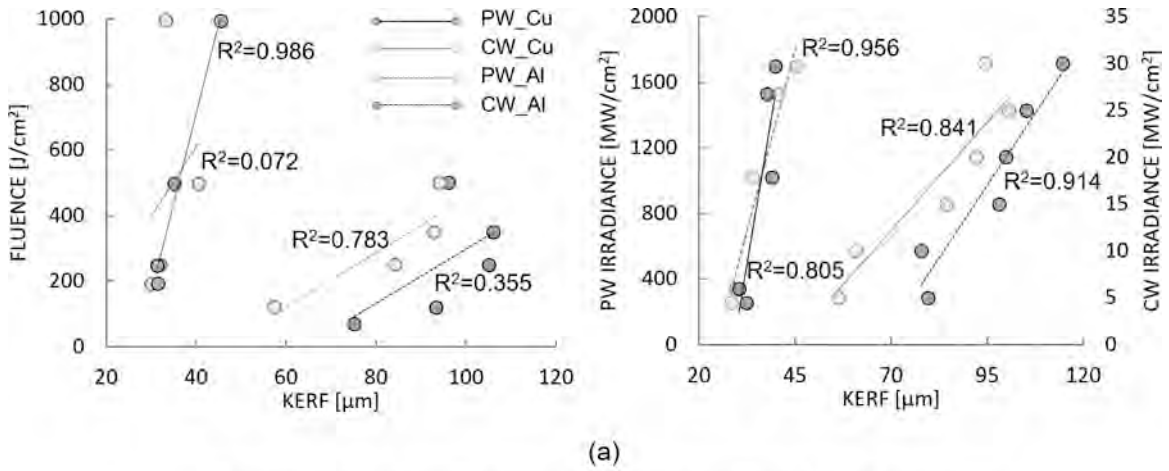

(a)

Cut condition - variable under consideration	R-squared value	Cut condition - variable under consideration	R-squared value
CW_Al - Fluence	0.355	CW_Al - Irradiance	0.914
PW_Al - Fluence	0.072	PW_Al - Irradiance	0.956
CW_Cu - Fluence	0.783	CW_Cu - Irradiance	0.841
PW_Cu - Fluence	0.986	PW_Cu - Irradiance	0.805

(b)

Fig. 15. Kerf-fluence and kerf-irradiance correlations with R-squared values. Trend lines (a) and summary of R-squared values (b).

trends were assumed. Fig. 15 displays the resulting trend lines and R-squared coefficients related to the accuracy of the regression line. These results demonstrate that the kerf width for aluminum foil was primarily correlated to the irradiance, while for copper foil it was connected to both irradiance and fluence. Considering the discussion points raised in Section 4.2, it is possible to infer that, for aluminum foil, the cut width depended on irradiance and power, while the HAZ depended on the fluence and interaction time.

5. Conclusion

State-of-the-art of laser cutting of aluminum and cooper current collectors of thickness 12 µm and 6 µm, respectively, has been presented in the context of battery electrode production. Continuous-wave and pulsed laser sources with high performance scanning heads were used for experiments, allowing investigation into how the laser source, material, and process parameters were correlated with the cut quality, kerf width and defect formation. The main outcome was that CW single mode fiber lasers enable higher cut quality under all tested conditions, surpassing the current state-of-the-art in metal foil cutting. Although both PW and CW setups led to similar process parameter windows achieving best cut quality, the CW setup achieved overall superior cut quality than the PW setup. The results showed that there were fewer or no burns, less spatter, and a more uniform kerf width geometry and re-solidified edges with a CW laser. Additionally, when comparing optimal process parameters for both setups, the quality was clearly better with the CW source. The only exception was low-speed ($\leq$ 4 m/s) cutting of copper foils. In this case, the resulting cut edge was jagged and irregular with the CW laser, whereas less significant dross and remelted edges were observed with the PW laser under low-speed cutting conditions with low irradiance ($<$ 350 MW/cm^2).

From a process parameter point of view, it was possible to achieve cutting speeds greater than 20 m/s with acceptable cut quality with both CW and PW laser sources. A maximum value of 28 m/s was attained with the CW laser source. Limitations in terms of cutting speeds greater than 28 m/s are currently related to the limitations of galvanometric scanning heads rather than available laser sources.

CRediT authorship contribution statement

Caterina Angeloni: Investigation. Writing - Review & Editing Erica Liverani: Methodology. Writing - Original Draft. Alessandro Ascari: Investigation. Alessandro Fortunato: Conceptualization. Writing - Review & Editing.

Declaration of Competing Interest

The authors declare that they have no known competing financial interests or personal relationships that could have appeared to influence the work reported in this paper.

Data Availability

Data will be made available on request.

References

Babadjanov, F., Specht, U., Lukasczyk, T., Mayer, B., 2023. Heat accumulation-induced surface structures at high degrees of laser pulse overlap on Ti6Al4V surfaces by femtosecond laser texturing. Materials 16 (6), 2498. https://doi.org/10.3390/ma16062498.

Banat, D., Ganguly, S., Meco, S., Harrison, P., 2020. Application of high power pulsed nanosecond fibre lasers in processing ultra-thin aluminium foils. Opt. Lasers Eng. 129, 106075 https://doi.org/10.1016/j.optlaseng.2020.106075.

Baumann, R., Lasagni, A.F., Herwig, P., Wetzig, A., Leyens, C., Beyer, E., 2019. Efficient separation of battery materials using remote laser cutting–high output performance, contour flexibility, and cutting edge quality. J. Laser Appl. 31, 022210 https://doi.org/10.2351/1.5096127.

Berhe, M.G., Oh, H.G., Park, S., Lee, D., 2022. Laser cutting of silicon anode for lithium-ion batteries. J. Mater. Res. Technol. 16, 322–334. https://doi.org/10.1016/j.jmrt.2021.11.135.

Jansen, T., Kandula, M.W., Blass, D., Hartwig, S., Haselrieder, W., Dilger, K., 2019. Evaluation of the separation process for the production of electrode sheets (Advances in Battery Cell Production). Energy Technol. 8 (2). https://doi.org/10.1002/ente.201900519.

Kim, H., Nam, K., Kim, Y., Ki, H., 2022. Analysis of laser-beam absorptance and keyhole behavior during laser keyhole welding of aluminum alloy using a deep-learning-based monitoring system. J. Manuf. Process. 80, 75–86. https://doi.org/10.1016/j.jmapro.2022.05.044.

Lee, D., 2018. Investigation of physical phenomena and cutting efficiency for laser cutting on anode for Li-ion batteries. Appl. Sci. 8 (2), 266. https://doi.org/10.3390/app8020266.

Lee, D., Mazumder, J., 2018. Effects of momentum transfer on sizing of current collectors for lithium-ion batteries during laser cutting. Opt. Laser Technol. 99, 315–325. https://doi.org/10.1016/j.optlastec.2017.09.016.

Lee, D., Patwa, R., Herfurth, H., Mazumder, J., 2012. Computational and experimental studies of laser cutting of the current collectors for lithium-ion batteries. J. Power Sources 210, 327–338. https://doi.org/10.1016/j.jpowsour.2012.03.030.

Lee, D., Oh, B., Suk, J., 2019. The effect of compactness on laser cutting of cathode for lithium-ion batteries using continuous fiber laser. Appl. Sci. 9 (1), 205. https://doi.org/10.3390/app9010205.

Luetke, M., Franke, V., Techel, A., Himmer, T., Klotzbach, U., Wetzig, A., Beyer, E., 2011. A comparative study on cutting electrodes for batteries with lasers. Phys. Procedia 12, 286–291. https://doi.org/10.1016/j.phpro.2011.03.135.

Lutey, A.H.A., Fiorini, M., Fortunato, A., Ascari, A., 2014. Chemical and microstructural transformations in lithium iron phosphate battery electrodes following pulsed laser exposure. Appl. Surf. Sci. 322, 85–94. https://doi.org/10.1016/j.apsusc.2014.10.069.

Lutey, A.H.A., Fortunato, A., Ascari, A., Carmignato, S., Leone, C., 2015. Laser cutting of lithium iron phosphate battery electrodes: characterization of process efficiency and quality. Opt. Laser Technol. 65, 164–174. https://doi.org/10.1016/j.optlastec.2014.07.023.

Mei, L., Lin, L., Yan, D., Xie, S., Liu, Y., Li, S., 2023. Metal spattering in laser scanning welding of T2 copper and welding quality. Opt. Lasers Eng. 161, 107392 https://doi.org/10.1016/j.optlaseng.2022.107392.

Pfleging, W., 2018. A review of laser electrode processing for development and manufacturing of lithium-ion batteries. Nanophotonics 7, 549–573. https://doi.org/10.1515/nanoph-2017-0044.

Schmieder, B., 2017. Laser cutting of graphite anodes for automotive lithium-ion secondary batteries: investigations in the edge geometry and heat affected zone. Proceding of SPIE 2012;8244:82440R-1–82440R-7.

Schulz, W., Kostrykin, V., Nießen, M., Michel, J., Petring, D., Kreutz, E.W., Poprawe, R., 1999. Dynamics of ripple formation and melt flow in laser beam cutting. J. Phys. D: Appl. Phys. 32, 1219. https://doi.org/10.1088/0022-3727/32/11/307.

Wandera, C., Salminen, A., Kujanpaa, V., 2009. Inert gas cutting of thick-section stainless steel and medium-section aluminum using a high power fiber laser. J. Laser Appl. 21, 154–171. https://doi.org/10.2351/1.3184429.

Wu, B., Yang, Y., Liu, D., Niu, C., Gross, M., Seymour, L., Lee, H., Le, P.M.L., Vo, T.D., Deng, Z.D., Dufek, E.J., Whittingham, M.S., Liu, J., Xiao, J., 2019. Good practices for rechargeable lithium metal batteries. J. Electrochem. Soc. 166 https://doi.org/10.1149/2.0691916jes.

Zhang, Y., Li, J., Rukun, Yang, Tongwei, Liu, Yiguo, Yan, 2019. Analysis of kerf quality on ultrafast laser cutting of anode material for lithium-ion battery. Opt. Lasers Eng. 118, 14–21. https://doi.org/10.1016/j.optlaseng.2019.01.013.